chemosensors

MDPI

Article

Preparation and Hydrogen-Sensitive Property of WO_3/Graphene/Pd Ternary Composite

Lin Wang [1,2], Fei An [2], Xinmei Liu [1,*], Dongzhi Zhang [3] and Zhe Yang [2,*]

[1] College of Chemistry and Chemical Engineering, China University of Petroleum (East China), Qingdao 266580, China; wangl.qday@sinopec.com
[2] State Key Laboratory of Safety and Control for Chemicals, SINOPEC Research Institute of Safety Engineering Co., Ltd., Qingdao 266071, China; anf.qday@sinopec.com
[3] College of Control Science and Engineering, China University of Petroleum (East China), Qingdao 266580, China; dzzhang@upc.edu.cn
* Correspondence: lxmei@upc.edu.cn (X.L.); yangzhe.qday@sinopec.com (Z.Y.); Tel.: +86-532-86980908 (X.L.); +86-532-83786640 (Z.Y.)

Abstract: Hydrogen (H_2) is a renewable energy source that has the potential to reduce greenhouse gas emissions. However, H_2 is also highly flammable and explosive, requiring sensitive and safe sensors for its detection. This work presents the synthesis and characterization of WO_3/graphene binary and WO_3/graphene/Pd (WG-Pd) ternary nanocomposites with varying graphene and Pd contents using the microwave-assisted hydrothermal method. The excellent catalytic efficacy of Pd nanoparticles facilitated the disintegration of hydrogen molecules into hydrogen atoms with heightened activity, consequently improving the gas-sensing properties of the material. Furthermore, the incorporation of graphene, possessing high conductivity, serves to augment the mobility of charge carriers within the ternary materials, thereby expediting the response/recovery rates of gas sensors. Both graphene and Pd nanoparticles, with work functions distinct from WO_3, engender the formation of a heterojunction at the interface of these diverse materials. This enhances the efficacy of electron–hole pair separation and further amplifies the gas-sensing performance of the ternary materials. Consequently, the WG-Pd based sensors exhibited the best gas-sensing performance when compared to anther materials, such as a wide range of hydrogen concentrations (0.05–4 vol.%), a short response time and a good selectivity below 100 °C, even at room temperature. This result indicates that WG-Pd ternary materials are a promising room-temperature hydrogen-sensing materials for H_2 detection.

Keywords: WO_3; graphene; Pd; microwave; hydrothermal; H_2; sensors; room temperature

Citation: Wang, L.; An, F.; Liu, X.; Zhang, D.; Yang, Z. Preparation and Hydrogen-Sensitive Property of WO_3/Graphene/Pd Ternary Composite. *Chemosensors* **2023**, *11*, 410. https://doi.org/10.3390/chemosensors11070410

Academic Editor: Michele Penza

Received: 12 June 2023
Revised: 10 July 2023
Accepted: 14 July 2023
Published: 21 July 2023

1. Introduction

Hydrogen, an eco-friendly and renewable energy source, has gained considerable interest in its wide range of applications, including automobile, fuel cell and space rocket applications [1,2]. However, hydrogen exhibits a colorless, odorless and explosive nature with a low ignition energy (0.02 mJ) and a wide flammable range of 4–74 vol.% in air, leading to many safety issues [3,4]. Therefore, rapid and accurate detection of hydrogen leakage is necessary for large-scale utilization of hydrogen. In recent years, chemiresistive hydrogen sensors based on metal oxide semiconductors (MOS), such as ZnO, SnO_2, MoO_3, WO_3, etc., have been widely applied to hydrogen detection due to their low cost, high sensitivity and short recovery time [5–8]. Among these MOS, WO_3, with its unique morphological structure, gasochromic properties, and high diffusion coefficient of oxygen vacancies, has proven to be one of the most attractive sensing materials [9]. However, the pure WO_3 sensors need a high working temperature (200–400 °C) to detect hydrogen, which may lead to power consumption and source of ignition [10,11].

Based on recent research findings, incorporating graphene or its derivatives (such as graphene oxide or reduced graphene oxide) has emerged as a promising strategy to lower

the operating temperature of MOS-based sensors. This is attributed to the remarkable properties of graphene, including excellent conductivity, high carrier mobility at room temperature, low electrical noise and a large surface area [12–14]. Moreover, graphene and its derivatives have various active sites (such as oxygen functional groups, defects, vacancies and π-π covalent bonds) that can selectively adsorb target gases, thereby enhancing the sensitivity and selectivity of the sensors. Furthermore, a heterogeneous structure (p–n or p-p junction) can be formed at the interface between graphene and metal oxides. This structure can facilitate the adsorption or resistance modulation of target gas molecules, which can improve the sensing performance of the material [15]. Consequently, chemiresistive sensors based on WO_3 sheets, hemispheres, aerogels, etc., combined with graphene have demonstrated lower working temperatures (<150 °C) towards target gases. For instance, Chu et al. reduced the optimal operating temperature of WO_3 from 180 °C to 100 °C by adding 0.1 wt% graphene [16]. Gui et al. fabricated hemispherical WO_3/graphene nanocomposites with hollow structures to achieve triethylamine sensing at room temperature [17]. Zhao et al. synthesized mesoporous WO_3@graphene aerogel nanocomposites, which exhibited a good response to acetone at 150 °C [18].

The hydrogen-sensing properties (e.g., sensitivity, response time and selectivity) of MOS can also be enhanced by decorating them with noble metals (such as Au, Ag, Pt or Pd). This enhancement results from the chemical and electronic sensitization of noble metals, where the former is achieved by the dissociation of hydrogen molecules and the latter by the change of electron depletion layers generated by heterogeneous structures [19]. Among these noble metals, Pd is considered to have the greatest effect on improving the hydrogen-sensing performance. It can spill over hydrogen molecules into atoms, which combine with Pd to form palladium hydride, resulting in a significant change in resistance. This reaction is reversible at room temperature. For example, Zhu et al. synthesized PdNPs@WO_3NPs, which showed a fast response (1.2 s) to hydrogen at 50 °C [20]. Le et al. fabricated a fast and efficient hydrogen gas sensor using $PdAu_{alloy}$@ZnO core–shell nanoparticles [21].

In this study, we examined the morphology and distribution of WO_3/graphene binary materials and WO_3/graphene/Pd ternary materials (WG-Pd) fabricated by microwave-assisted hydrothermal method. The structure of both binary and ternary materials was influenced by the content of graphene and Pd. Moreover, we investigated the relationship between the content of graphene in WO_3/graphene binary materials and their hydrogen-sensing properties to determine the optimal graphene content for hydrogen sensing. Additionally, we evaluated the working temperature, repeatability and selectivity of WG-Pd ternary materials. Finally, we discussed the sensing mechanism of WG-Pd.

2. Materials and Methods

2.1. Materials

GO suspension (GO-1, Hangzhou Gaoxi Technology Co., Ltd, Hangzhou, China); absolute ethanol (99.7%, Sinopharm, Shanghai, China); HCl (99.5%, Sinopharm, Shanghai, China); Na_2WO_3 (Sigma-Aldrich, St. Louis, MO, USA); $PdCl_2$ (Sigma-Aldrich, St. Louis, MO, USA). All reagents were of analytical grade without further purification, and the deionized water was used in all experiments.

2.2. Fabrication of WO_3/Graphene/Pd Ternary Materials

A certain amount of GO was dispersed in 190 mL deionized water followed by ultrasonication. Next, 1.06 g of Na_2WO_3 was added into GO dispersion, and 50 mL of HCl (2 M) was added drop-by-drop into the mixture under vigorous stirring for 30 min. The suspension was poured into autoclaves and subjected to microwave heating at 180 °C for 1 h using a Multiwave PRO oven (Anton Paar, Graz, Austrian). The precipitate was then collected and washed by centrifugation in deionized water and absolute ethanol, followed by freeze-drying under vacuum at room temperature. The WO_3/graphene nanomaterials were synthesized with different GO/WO_3 mass ratios of 0.5, 1, 2 and 3:50, and denoted as W0.5G, WG, W2G and W3G, respectively. Pure WO_3 was also prepared in the same

way without GO for comparison. A quantity of 50 mg of WG and a specific amount of $PdCl_2$ were dispersed in 5 mL of absolute ethanol using ultrasonication for a duration of 30 min. The resulting mixture was then dried in an oven at a temperature of 80 °C for a period of 12 h, followed by thermal annealing in a nitrogen atmosphere at a temperature of 300 °C for 2 h. The samples obtained from this process, with $PdCl_2$ masses of 1, 5 and 10 mg, respectively, were designated as WG-1Pd, WG-5Pd and WG-10Pd.

2.3. Characterization

Scanning electron microscopy (SEM, JEOL JSM-7610F, Tokyo, Japan) and transmission electron microscopy (TEM, FEI Talos, Columbia, SC, USA) were used to observe the morphologies of ternary nanomaterials. The phases of samples were analyzed by X-ray diffraction (XRD, Bruker D8 Advance, Billerica, MA, USA). The chemical compositions of ternary nanomaterials were measured using Thermo Fisher (Waltham, MA, USA) ESCALAB 250 XI X-ray photoelectron spectroscopy (XPS).

2.4. Fabrication and Test of Gas Sensors

The WG and WG-Pd powders were blended with terpineol in a 1:2 mass ratio, while finely grinding them in a mortar. The resultant paste was uniformly coated on an Al_2O_3 tube with a pair of Pt wires. To heat the gas sensor, a Ni-Cr heating wire was inserted into the tube. The sensors were pre-treated at 100 °C for 5 days to enhance their stability before the tests. The gas-sensing measurements were carried out using a CGS-8 Gas Sensing Measurement System (Beijing Elite Tech Company Limited, Beijing, China) with a 500 mL test chamber. The sensors' resistance was stabilized at the desired temperature before a known volume of gas was injected into the chamber. The tests were performed under ambient conditions of 25 ± 5 °C and 40 ± 5% relative humidity.

The gas response was calculated as $(R_{air} - R_{gas})/R_{air}$, where R_{air} and R_{gas} are the sensor resistance in air and target gas, separately. The response time and recovery time are the time intervals required for the sensor response to reach 90% of its total change upon exposure to the target gas or air, respectively.

3. Results

3.1. Morphology and Structure

In order to characterize the surface morphology and distribution of WO_3, WG and WG-Pd, SEM and EDS were utilized. As shown in Figure 1a, WO_3 obtained by the microwave-assisted hydrothermal method showed a nanoribbon-like structure with a length of about 200 nm and a thickness of about 30 nm. The two-dimensional structure had a high surface-to-volume ratio and abundant surface functional groups, which offer a large number of adsorption sites for the target gas and oxygen molecules. This leads to effective physisorption and chemisorption of gas molecules at low temperature. Hence, two-dimensional materials have some advantages in providing fast and complete diffusion of H_2 gas throughout the structure and are widely used as gas-sensing materials [22–24]. Following the incorporation of GO, WG was interconnected by delicate folded RGO layers amid multiple WO_3 nanoribbons. The folded configuration of RGO primarily resulted from lamellar distortion induced by partial reduction of GO during the microwave-assisted hydrothermal process (Figure 1b–e) [25,26]. In the case of W0.5G with a lower graphene content, only a limited number of WO_3 nanoribbons were linked by graphene (Figure S1a). Conversely, with a higher graphene content in W2G, a significantly larger proportion of WO_3 nanoribbons were connected by graphene, albeit some were enveloped by it (Figure S1b). As the graphene content increased, porous structures gradually formed within the composite due to graphene stacking, enveloping the WO_3 nanoribbons and leaving only a few exposed (Figure S1c). Subsequent to Pd loading onto the surface of WG, a substantial amount of Pd was uniformly distributed, as evidenced by the EDS image (Figure 1f–h).

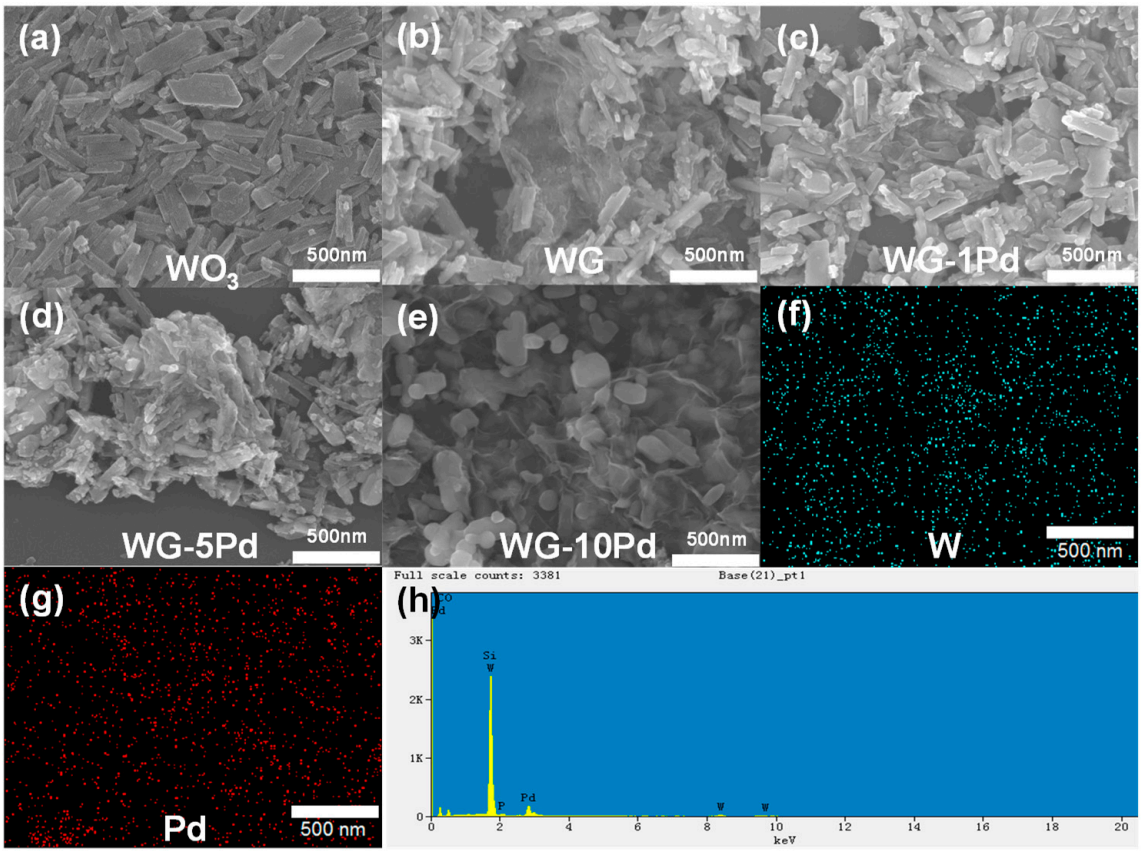

Figure 1. (**a**–**e**) SEM images of WO_3, WG and WG-Pd, (**f**–**h**) corresponding EDS elemental mapping and EDS spectra of WG-10Pd.

The hierarchical structures of WG and WG-Pd were characterized by TEM. As shown in Figure 2a–c, in addition to large nanoribbons, there were a few nanosheets of WO_3 around 10–20 nm of WG, which should be grown on the surface of graphene. There were a few nanosheets of WO_3 of around 10–20 nm on the surface of WG, indicating that they were grown on the graphene surface. After loading Pd onto WG, spherical Pd nanoparticles appeared on the surface of graphene (Figure 2d–f). With a Pd content of 1%, Pd nanoparticles were sporadically distributed on graphene nanosheets with a size of 3 nm. When increasing the Pd content, the number and size of Pd nanoparticles also increased. When the Pd content increased to 10%, Pd nanoparticles were more densely distributed and had a larger size of 10 nm. Moreover, even for the WG-Pd with the highest content of Pd, no significant aggregation of Pd nanoparticles was observed. This phenomenon stemmed from the mutual interaction between the abundant oxygen-containing functional groups on the surface of graphene oxide and Pd ions, which led to their adsorption and uniform growth on the surface of graphene nanoflakes and prevented the aggregation of Pd nanoparticles. This phenomenon can be attributed to the interaction between the abundant oxygen-containing functional groups on the surface of graphene oxide and Pd ions. This interaction leads to the adsorption and uniform growth of Pd nanoparticles on the surface of graphene nanoflakes, preventing their aggregation.

Figure 3 shows XRD patterns of WO_3 and WG-Pd. WO_3 exhibited distinct diffraction peaks of orthorhombic phase of $WO_3 \cdot 0.33H_2O$ (JCPDS 72-199) [27,28], indicating the presence of crystal H_2O before thermal annealing. For the WO_3/graphene composite nanomaterials, the characteristic peaks at 22.7°, 28.1°, 36.5°, 49.9° and 55.3° were slightly different from those of pure-phase WO_3. This was attributed to the interaction between the functional groups (hydroxyl, carbonyl and carboxyl groups) on the graphene surface and Na_2WO_3, which influenced the WO_3 growth. Moreover, slight deviation from stoichiome-

try (WO_{3-x}) could also affect the peak position. They also exhibited a broad characteristic peak around 20°, which was caused by the imperfect restacking due to the curvature of graphene sheets [29] (Figure S2). After loading with Pd and thermal annealing, WG-1Pd, WG-5Pd and WG-10Pd had different XRD patterns with WG. As shown in Figure 3b–d, there were diffraction features matching hexagonal phase of WO_3 due to the dehydration after annealed [30]. Furthermore, characteristic peaks of Pd (JCPDS 46-1043) and PdO (JCPDS 43-1024) appeared in WG-Pd, applying the presence of Pd and PdO attributed to the particle oxidization of Pd nanoparticles in air [31].

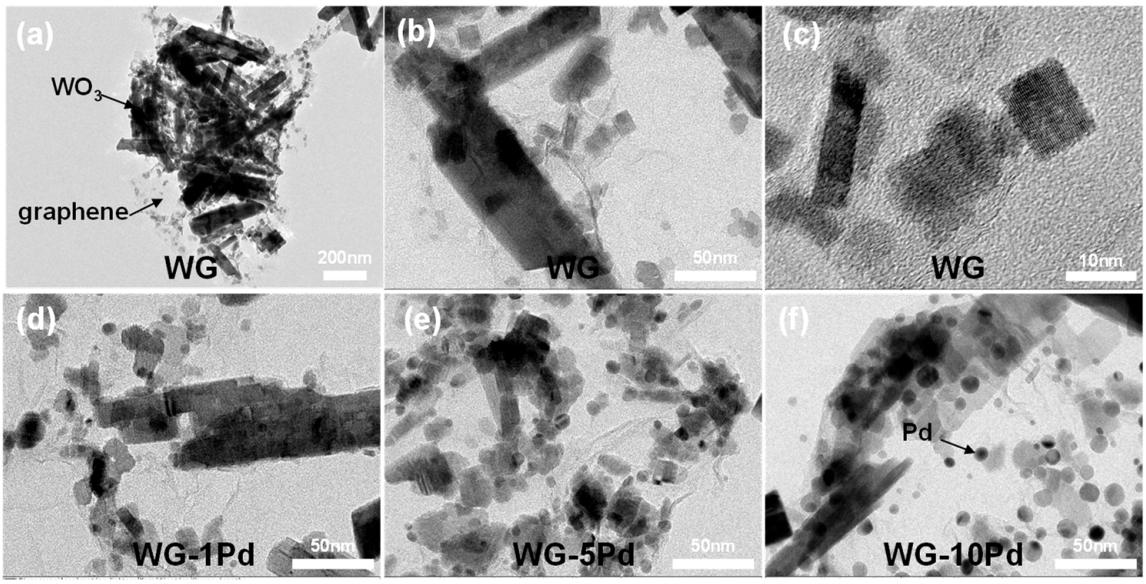

Figure 2. TEM images of (**a**–**c**) WG and (**d**–**f**) WG-Pd.

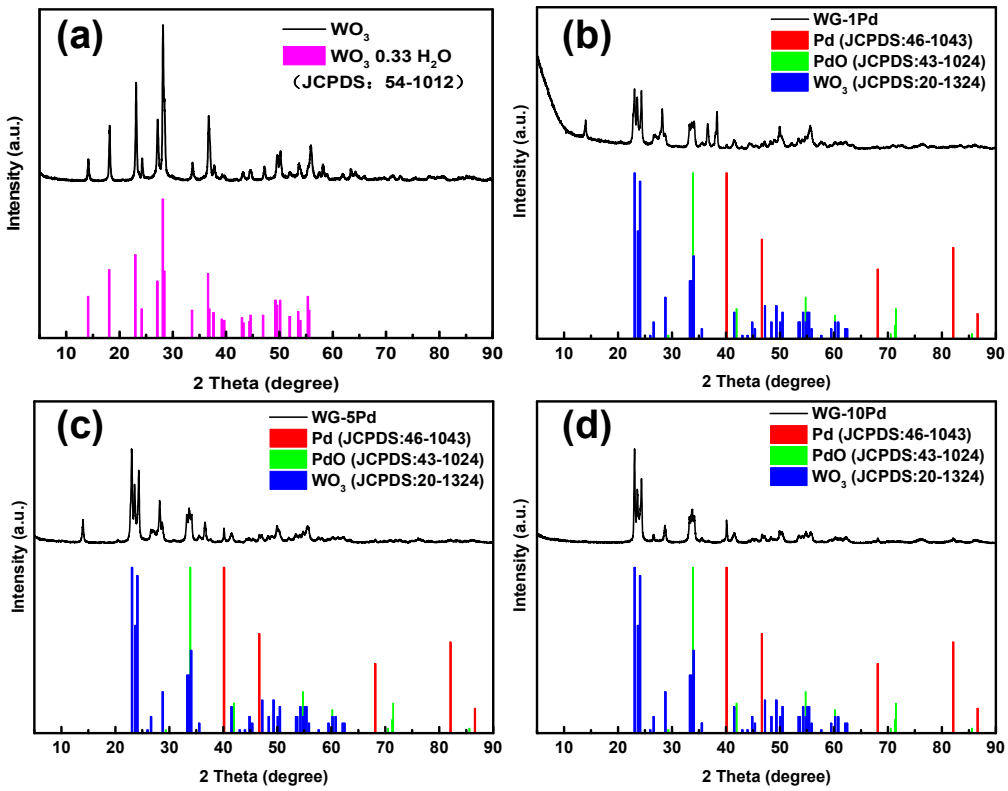

Figure 3. XRD patterns of (**a**) WO_3 and (**b**–**d**) WG-Pd.

In order to accurately analyze the content and valence state of elements in WG-10Pd, XPS analysis was utilized (Figure 4). As shown in Figure 4a, the material was mainly composed of W, C, O and Pd. Figure 4b demonstrates the deconvoluted Pd (3d) XPS spectra of WG-10Pd. It can be found that Pd element was mainly metallic Pd^0 located at 335.3 and 340.55 eV. Additionally, there were other peaks of oxidized Pd^{2+} located at 336.6 and 341.85 eV and Pd^{4+} located at 338.2 and 343.45 eV [32]. This also corresponds to the XRD spectra. A small amount of oxidized Pd came from the partial oxidation of surface atoms of Pd nanoparticles by air due to their high activity.

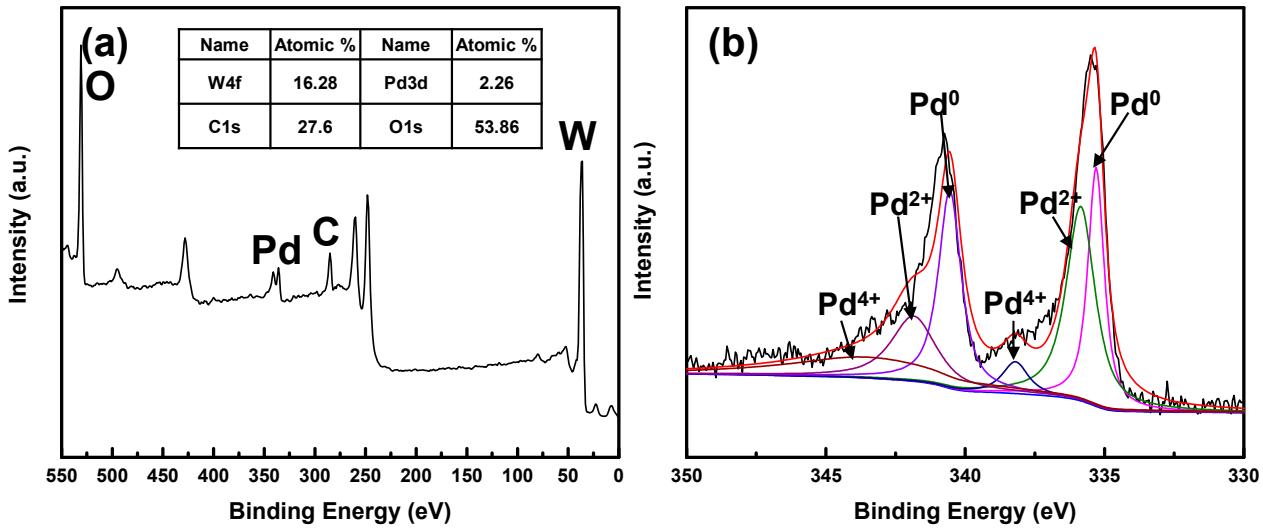

Figure 4. (**a**) XPS survey of WG-10Pd; (**b**) high-resolution XPS spectra of Pd 3d of WG-10Pd.

3.2. Hydrogen Gas Sensing

The effects of graphene content and working temperature on the hydrogen response performance of WO_3/graphene nanomaterials are shown in Figure 5. As can be seen from Figure 5a, at 50 °C, WO_3, W0.5G and W3G had no response to hydrogen. Among them, WO_3 and W0.5G had large resistances (7130 MΩ and 2500 MΩ, respectively) that exceeded the instrument resistance range (500 MΩ) and could not be measured. This was because WO_3, as a metal oxide semiconductor, had a large resistance at low temperatures, and even with a small amount of graphene added, it still could not meet the measurement requirements. WG had the best response performance, but due to the low working temperature, it only responded to hydrogen concentrations above 0.4%. Although W2G and W3G had higher graphene contents than WG, their response performance was reduced. This was attributed to the excess graphene that could cover or even wrap around WO_3 and provide an additional path for current flow, resulting in a significant increase of the conductivity of the sample, which made resistance variation in reducing environment less noticeable. As the working temperature increased to 100 °C and 150 °C, the response performance of WG, W2G and W3G were all improved. The response of WG, W2G and W3G to 1% H_2 at 100 °C was 30.8, 28.9 and 2.5%, respectively. After heating at 150 °C, the corresponding responses increased to 90.5, 56.3 and 7.9%, respectively. This result indicated that WG had the highest response performance. At the same time, as the working temperature increased from 50 °C to 150 °C, WG's response time to 1% hydrogen was shortened from 223 s to 67 s (Figure 5d,e). Meanwhile, WG showed p-n switching phenomenon at different temperatures, which was mainly caused by the combination of different semiconductor materials and the change of charge transfer path at different working temperatures. Graphene (p-type semiconductor) and WO_3 (n-type semiconductor) formed a composite, in which the carriers of both graphene and WO_3 participated in the conduction path, showing a mixed p-n characteristic. At low temperature, WO_3 transferred electrons to GO, showing p-type behavior. At high temperature, WO_3 received electrons from GO, showing n-type

behavior. However, WG still had no response to hydrogen at room temperature and needed to be composited with Pd to further improve its response performance. Therefore, we used WG as the base material and composite different contents of Pd nanoparticles to study the effects of Pd content and working temperature on the hydrogen response performance.

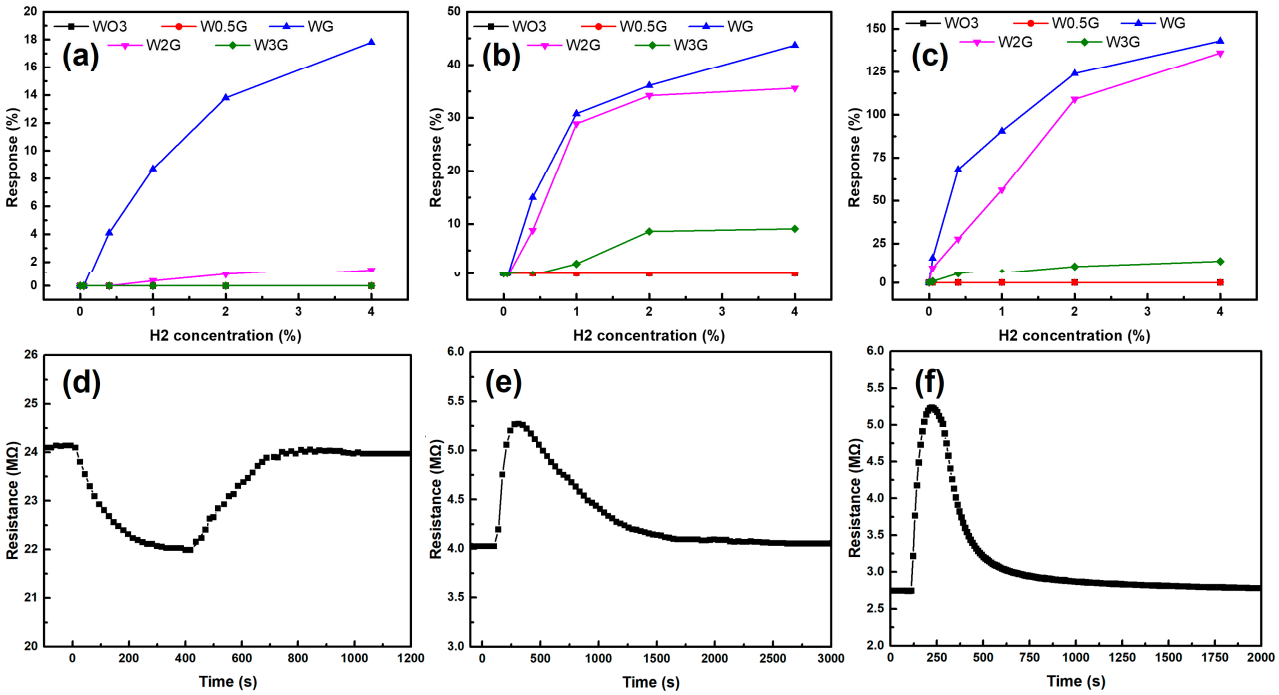

Figure 5. The response of WO_3/graphene nanomaterials at 50 (**a**), 100 (**b**) and 150 °C (**c**); The resistance of WG for 1% H_2 at 50 (**d**), 100 (**e**) and 150 °C (**f**).

The effect of Pd content and working temperature was studied by testing these gas sensors at different temperature ranging from 25 to 100 °C as shown in Figure 6. For WG-1Pd and WG-5Pd, there was no evident response to 500 ppm of H_2 at 25 °C, applying low content of Pd was not sufficient for H_2 sensing at room temperature. However, WG-10Pd with larger content of Pd showed response to 500 ppm of H_2 at 25 °C with value of 2.3%. WG-1Pd, WG-5Pd and WG-10Pd were more sensitive to H_2 at higher working temperature. The response to 500 ppm H_2 of WG-1Pd, WG-5Pd and WG-10Pd increased to 86.1%, 92.6% and 94.6% at a working temperature of 100 °C, respectively. This phenomenon stemmed from the lower gas activation energy of adsorption/desorption at higher temperature. Meanwhile, WG-10Pd still showed a higher response to H_2 than the others. Compared with the WO_3/graphene binary materials without Pd, the hydrogen-sensing performance of the WO_3/graphene/Pd ternary composite improved significantly. WG exhibited no noticeable response to 500 ppm hydrogen, while the response value increased to 86.1% with the addition of 1% Pd nanoparticles, indicating that Pd had a remarkable effect on enhancing the hydrogen response.

The dynamic response of WG-10Pd was studied at various H_2 concentrations (ranging from 0.05–4%) and at temperatures of 25, 50, 75 and 100 °C. As shown in Figure 7a, WG-10Pd showed excellent response to hydrogen in the range of 0.05–4% at room temperature. The response value increased gradually with the increase of the concentration of H_2. At 4% of H_2, the response value reached 96.1%. On the contrary, the response time was gradually shortened. The response time was reduced to within 40 s at 4% of H_2. After heating to 50, 75 and 100 °C, the response value was further improved and the response time was shorter. At 100 °C, the response value of 0.05% H_2 could reach 94.6%, and the response time was shortened to 6 s. However, the response curves reached a plateau at relatively low concentrations, proving its insensitivity to high concentration of H_2. Therefore, WG-10Pd

was more suitable for the measurement of low-concentration hydrogen below 0.05% after heating. The saturation phenomenon was ascribed to the increased catalytic effect of Pd at high temperature, which generated abundant chemisorbed water and occupied the active sites for oxygen adsorption.

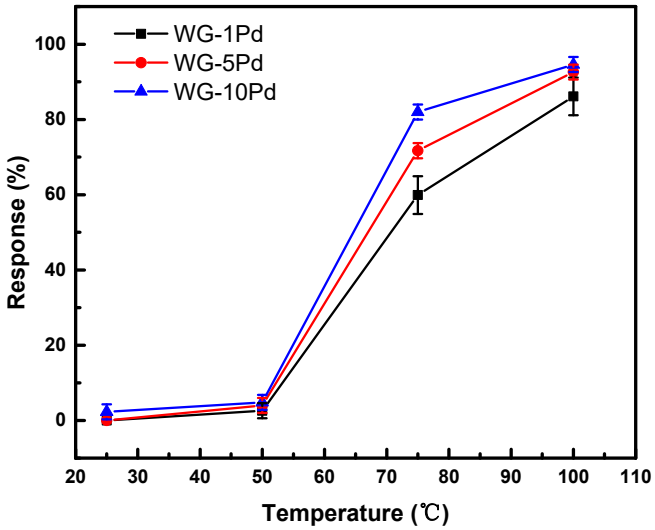

Figure 6. The response of WG-Pd for 500 ppm H_2 at different temperatures ranging from 25 to 100 °C.

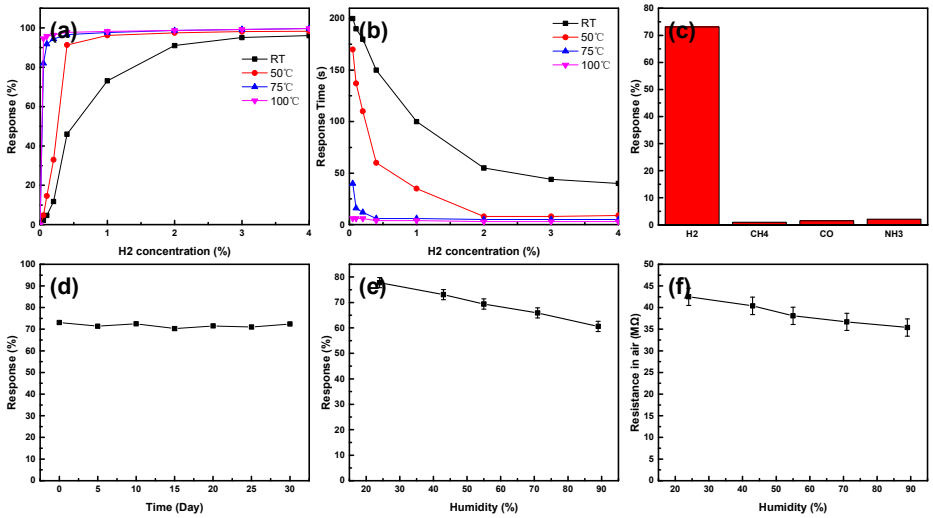

Figure 7. (**a**) The response value and (**b**) response time of WG-10Pd to 0.05–4% H_2 at different temperature ranging from 25 to 100 °C; (**c**) the response of WG-10Pd to 1% H_2, CH_4, CO and NH_3; (**d**) the response of WG-10Pd to 1% H_2 for 30 days; (**e**) the response and (**f**) the resistance in air of WG-10Pd under different RH.

WG-10Pd hydrogen-sensing material had excellent selectivity and stability. As demonstrated in Figure 7c, the response value of WG-10Pd to 1% H_2 at room temperature was significantly higher than that of CH_4, CO and NH_3 with the same concentration, showing high selectivity of H_2, due to the catalytic properties of Pd to hydrogen dissociation. After 30 days of uninterrupted testing, the change of response value was still maintained within 5%, implying the high stability of WG-10Pd.

The effect of relative humidity (RH) on the sensing performance of WG-10Pd at room temperature was also investigated. Figure 7e,f shows that the response of WG-10Pd decreased with increasing RH. This phenomenon was caused by the water vapor occupying the adsorption sites and hindering the oxygen adsorption. The response values of WG-10Pd

to 1% H_2 were 77.8%, 73.1%, 69.4%, 65.9% and 60.6% under 24%, 43%, 55%, 71% and 89% RH, respectively. The response variation (calculated as 1 − Response (89RH%)/Response (24RH%)) was 22%, indicating that RH had a significant influence on the hydrogen sensing. Meanwhile, the resistance in air decreased from 42.5 to 35.4 MΩ as RH changed from 24% to 89%. Therefore, the resistance variation was about 16.7%.

Similarly, the response of WG-1Pd and WG-5Pd at 50–100 °C were studied (Figure 8). The variation trend of response value and response time was basically the same as that of WG-10Pd, but the response value was slightly reduced and the response time was extended. The responses to 0.05% H_2 at 100 °C of WG-1Pd and WG-5Pd were 86.1% and 92.6%, respectively, while the response times were 25 s and 9 s, respectively.

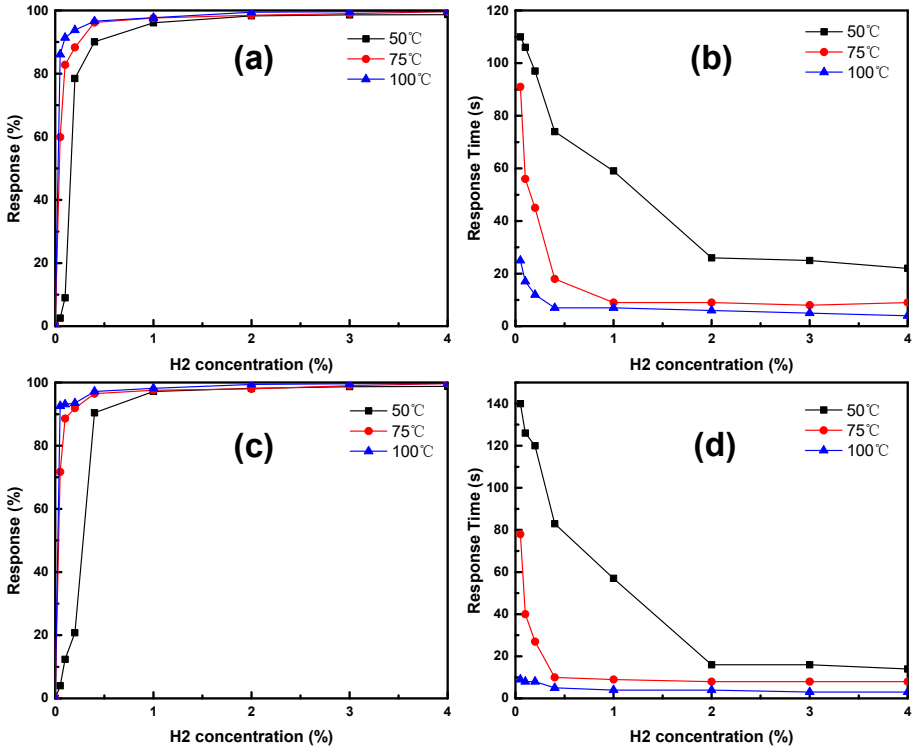

Figure 8. (**a**) The response value and (**b**) response time of WG-1Pd to 0.05–4% H_2 at different temperature ranging from 25 to 100 °C; (**c**) the response value and (**d**) response time of WG-5Pd to 0.05–4% H_2 at different temperatures ranging from 25 to 100 °C.

4. Discussion

The WG-Pd ternary materials had a good response to H_2 from room temperature to 100 °C due to their chemical composition and morphological structure (Figure 9). According to the surface depletion layer model, when the material contacts oxygen in the air, it forms oxygen negative ions (O_{2^-}, O^-, O^{2-}, etc.) on the surface by adsorbing electrons [33]. This increases electrical resistance. At different temperatures, oxygen anions have different valence states. Below 100 °C, it is mainly O_2^- ions. Between 100–300 °C, O^- dominates. Above 300 °C, oxygen anions are mostly O^{2-} [34,35]. Thus, the adsorbed oxygen ions on the surface of WG-Pd material are mainly O_2^-, as the operating temperature is below 100 °C. When it contacts hydrogen, O_2^- reacts with hydrogen to form water vapor and releases electrons to the material, causing a drop in resistance [36]. The resistance decrease is proportional to the hydrogen concentration, allowing measurement of hydrogen concentration through resistance change. The reaction process is as follows:

$$2H_2 + O_2^- \rightarrow 2H_2O + e^- \quad (1)$$

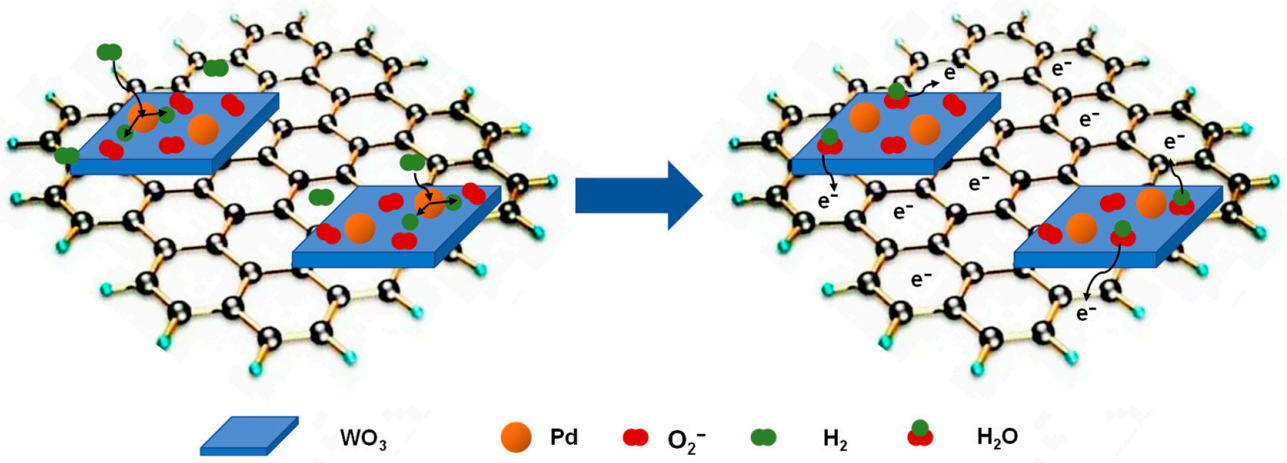

Figure 9. The schematic illustration of WG-Pd during exposure to H_2.

In the WG-Pd ternary composites, the three components showed different functions. As the material with the highest content, WO_3 played the main role in gas sensing. The abundant oxygen defects on its surface provided active sites for oxygen adsorption [37]. Pd nanoparticles could dissociate H_2 molecules into highly active hydrogen atoms, thus accelerating the reaction of O^{2-} with H_2. H_2 could also be directly dissolved into metal Pd to form Pd-H complex, thus significantly reducing the Schottky barrier on WO_3-Pd interface, enabling more electrons to enter the conduction band of the material and improving the electrical conductivity of the material [6]. However, electron transfer between different WO_3/Pd nanosheets was still hindered by the Schottky barrier between interfaces, while graphene sheets could significantly reduce that, providing multiple paths for electron transfer, thus further reducing the resistance [38]. Graphene itself had a high specific surface area and oxygen-containing functional groups, which improved response performance [39]. Moreover, the hydrogen-sensing performance could also be enhanced by the heterogeneous structure formed at the interface between graphene and WO_3. WO_3 is an n-type semiconductor material with more electrons than holes as the main carriers. Graphene sheets are p-type semiconductor materials with more holes than electrons as the main carriers, due to the intrinsic properties of graphene. Thus, there are many heterojunctions (p-n junctions) at the interface between p-type graphene and n-type WO_3. Because of the different work functions of graphene and WO_3, the holes transfer from graphene to WO_3 and the electrons transfer from WO_3 to graphene at the p-n junction. After the carrier exchange, the holes and electrons with opposite charges recombine. This leads to the decrease of concentration of effective carriers and formation of electron depletion layer and hole depletion layer at the interface of WO_3 and graphene, respectively. The depletion layer can increase the resistance of WG-Pd ternary composites in air and facilitate the adsorption or resistance modulation of H_2 gas molecules, which can improve the hydrogen-sensing properties at room temperature. Through the synergistic effect among the three components of WG-Pd, a sensitive response to hydrogen is achieved at temperatures lower than 100 °C.

5. Conclusions

In this paper, we fabricated WO_3/graphene binary materials and WG-Pd ternary materials with different contents of graphene and Pd using the microwave-assisted hydrothermal method. The sensing results showed that WG with 1% graphene exhibited the best hydrogen performance at 100 and 150 °C compared to other WO_3/graphene binary materials with different contents of graphene. However, WG still exhibited no noticeable response to hydrogen below 100 °C. For WG-Pd ternary materials, WG-10Pd showed the highest response to H_2 at room temperature. Moreover, it showed a wide range of hydrogen concentrations (0.05–4 vol.%), a short response time (40 s) and a good selectivity. Its sensing properties were further enhanced after heating to 50, 75 and 100 °C. The excellent sensing

properties resulted from the synergistic effect among the three components of WG-Pd. In summary, WG-Pd ternary materials are promising sensing materials for detection of H_2 leakage at temperatures lower than 100 °C, even at room temperature.

Supplementary Materials: The following supporting information can be downloaded at: https://www.mdpi.com/article/10.3390/chemosensors11070410/s1, Figure S1: SEM images of (a) W0.5G, (b) W2G and (c) W3G; Figure S2: XRD patterns of (a) W0.5G, (b) WG, (c) W2G and (d) W3G.

Author Contributions: Conceptualization, L.W.; methodology, F.A.; software, F.A.; validation, F.A.; formal analysis, L.W.; investigation, L.W.; resources, Z.Y.; data curation, F.A.; writing—original draft preparation, L.W.; writing—review and editing, L.W.; visualization, F.A.; investigation, formal analysis, supervision, X.L. and D.Z.; project administration, L.W.; investigation, methodology, supervision, funding acquisition, Z.Y. All authors have read and agreed to the published version of the manuscript.

Funding: This research was funded by The National Natural Science Foundation of China (52003297) and the National Key R&D Program of China (2022YFB3205504).

Institutional Review Board Statement: Not applicable.

Informed Consent Statement: Not applicable.

Data Availability Statement: All data supporting the conclusions of this article are included within this article.

Conflicts of Interest: The authors declare no conflict of interest.

References

1. Jabbr, A.I.; Gaja, H.; Koylu, U.O. Multi-objective optimization of operating parameters for a H_2/diesel dual-fuel compression-ignition engine. *Int. J. Hydrogen Energy* **2020**, *45*, 19965–19975. [CrossRef]
2. Robledo, C.B.; Leeuwen, L.; Wijk, A. Hydrogen fuel cell scooter with plug-out features for combined transport and residential power generation. *Int. J. Hydrogen Energy* **2019**, *44*, 29648–29657. [CrossRef]
3. Wang, F.; Hu, K.; Liu, H.; Zhao, Q.; Zhang, Y. Low temperature and fast response hydrogen gas sensor with Pd coated SnO_2 nanofiber rods. *Int. J. Hydrogen Energy* **2020**, *45*, 7234–7242. [CrossRef]
4. Zhang, Z.; Yin, C.; Yang, L.; Jia, W.; Zhou, J.; Xu, H.; Cao, D. H_2 response characteristics for sol–gel-derived WO_3-SnO_2 dual-layer thin films. *Ceram. Int.* **2017**, *43*, 6693–6699. [CrossRef]
5. Cheng, I.K.; Lin, C.Y.; Pan, F.M. Gas sensing behavior of ZnO toward H_2 at temperatures below 300 °C and its dependence on humidity and Pt-decoration. *Appl. Surf. Sci.* **2021**, *541*, 148551. [CrossRef]
6. Cai, Z.; Park, S. Synthesis of Pd nanoparticle-decorated SnO_2 nanowires and determination of the optimum quantity of Pd nanoparticles for highly sensitive and selective hydrogen gas sensor. *Sens. Actuators B Chem.* **2020**, *322*, 128651. [CrossRef]
7. Xu, K.; Liao, N.; Xue, W.; Zhou, H. First principles investigation on MoO_3 as room temperature and high temperature hydrogen gas sensor. *Int. J. Hydrogen Energy* **2020**, *45*, 9252–9259. [CrossRef]
8. Rahmani, M.B.; Yaacob, M.H.; Sabri, Y.M. Hydrogen sensors based on 2D WO_3 nanosheets prepared by anodization. *Sens. Actuators B Chem.* **2017**, *251*, 57–64. [CrossRef]
9. Chen, M.; Zou, L.; Zhang, Z.; Shen, J.; Li, D.; Zong, Q.; Gao, G.; Wu, G.; Shen, J.; Zhang, Z. Tandem gasochromic-Pd-WO_3/graphene/Si device for room-temperature high-performance optoelectronic hydrogen sensors. *Carbon* **2018**, *130*, 281–287. [CrossRef]
10. Boudiba, A.; Zhang, C.; Umek, P.; Bittencourt, S.R.; Olivier, M.G.; Debliquy, M. Sensitive and rapid hydrogen sensors based on Pd-WO_3 thick films with different morphologies. *Int. J. Hydrogen Energy* **2013**, *38*, 2565–2577. [CrossRef]
11. Mozalev, A.; Calavia, R.; Vazquez, R.M.; Grdcia, I.; Cane, C.; Correig, X.; Vilanova, X.; Gispert-Guirado, F.; Hubalek, J.; Llobet, E. Mems-microhotplate-based hydrogen gas sensor utilizing the nanostructured porous-anodic-alumina-supported WO_3 active layer. *Int. J. Hydrogen Energy* **2013**, *38*, 8011–8021. [CrossRef]
12. Tung, T.T.; Nine, M.J.; Krebsz, M.; Pasinszki, T.; Coghlan, C.J.; Tran, D.; Losic, D. Recent advances in sensing applications of graphene assemblies and their composites. *Adv. Funct. Mater.* **2017**, *27*, 1702891. [CrossRef]
13. Sajjad, S.; Leghari, S.; Iqbal, A. Study of graphene oxide structural features for catalytic, antibacterial, gas sensing and metals decontamination environmental applications. *ACS Appl. Mater. Interfaces* **2017**, *9*, 43393–43414. [CrossRef]
14. Chatterjee, S.G.; Chatterjee, S.; Ray, A.K.; Chakraborty, A.K. Graphene–metal oxide nanohybrids for toxic gas sensor: A review. *Sens. Actuators B Chem.* **2015**, *221*, 1170–1181. [CrossRef]
15. Lonkar, S.; Singh, K.K.; Swaminathan, S.; Abdala, A. Recent advances in graphene based gas sensors. *Sens. Actuators B Chem.* **2015**, *218*, 160–183.
16. Chu, X.; Tao, H.; Feng, G.; Dong, Y.; Sun, W.; Bai, L. Gas sensing properties of graphene–WO_3 composites prepared by hydrothermal method. *Mater. Sci. Eng. B* **2015**, *193*, 97–104. [CrossRef]

17. Gui, Y.; Zhao, J.; Wang, W.; Tian, J.; Zhao, M. Synthesis of hemispherical WO_3/graphene nanocomposite by a microwave-assisted hydrothermal method and the gas-sensing properties to triethylamine. *Mater. Lett.* **2015**, *155*, 4–7. [CrossRef]
18. Tao, Z.; Yuan, R.; Jia, G.; Zhao, Y.; Fan, Y.; Yang, J.; Zhang, X.; Jiang, W.; Wang, L.; Luo, W. Facile synthesis of mesoporous WO_3 @graphene aerogel nanocomposites for low-temperature acetone sensing. *Chin. Chem. Lett.* **2019**, *30*, 2032–2038.
19. Hashtroudi, H.; Atkin, P.; Mackinnon, I.; Shafiei, M. Low-operating temperature resistive nanostructured hydrogen sensors. *Int. J. Hydrogen Energy* **2019**, *44*, 26646–26664. [CrossRef]
20. Zhu, Z.; Xing, X.; Feng, D.; Li, Z.; Tian, Y.; Yang, D. Highly sensitive and fast-response hydrogen sensing of WO_3 nanoparticles via palladium reined spillover effect. *Nanoscale* **2021**, *13*, 12669–12675. [CrossRef]
21. Le, H.J.; Dao, D.V.; Yu, Y.T. Superfast and efficient hydrogen gas sensor using Pd Au alloy@ZnO core–shell nanoparticles. *J. Mater. Chem. A* **2020**, *8*, 12968–12974. [CrossRef]
22. Yang, S.; Wang, Z.; Zou, Y.; Luo, X.; Pan, X.; Zhang, X.; Hu, Y.; Chen, K.; Huang, Z.; Wang, S.; et al. Remarkably accelerated room-temperature hydrogen sensing of MoO_3 nanoribbon graphene composites by suppressing the nanojunction effects. *Sens. Actuators B Chem.* **2017**, *248*, 160–168. [CrossRef]
23. Yang, S.; Zhao, W.; Hu, Y.; Luo, X.; Gu, H. Highly responsive room-temperature hydrogen sensing of α-MoO_3 nanoribbon membranes. *ACS Appl. Mater. Interfaces* **2015**, *7*, 9247–9253. [CrossRef]
24. Kwak, T.D.; Wang, M.; Koski, K.J.; Zhang, L.; Lei, Y. Molybdenum trioxide (α-MoO_3) nanoribbons for ultrasensitive ammonia (NH_3) gas detection: Integrated experimental and density functional theory simulation studies. *ACS Appl. Mater. Interfaces* **2019**, *11*, 10697–10706. [CrossRef]
25. Peng, F.; Wang, S.; Yu, W.; Huang, T.; Dai, N. Ultrasensitive ppb-level H_2 gas sensor at room temperature based on WO_3/rGO hybrids. *J. Mater. Sci. Mater. Electron.* **2020**, *31*, 5008–5016. [CrossRef]
26. Hu, K.; Xie, X.; Szkopek, T.; Cerruti, M. Understanding hydrothermally reduced graphene oxide hydrogels: From reaction products to hydrogel properties. *Chem. Mater.* **2016**, *13*, 1756–1768. [CrossRef]
27. Perfecto, T.M.; Zito, C.A.; Volanti, D.P. Room-temperature volatile organic compounds sensing based on $WO_3 \cdot 0.33H_2O$, hexagonal-WO_3, and their reduced graphene oxide composites. *RSC Adv.* **2016**, *6*, 105171–105179. [CrossRef]
28. Perfecto, T.M.; Zito, C.; Mazon, T.; Volanti, D.P. Flexible room-temperature volatile organic compound sensors based on reduced graphene oxide–$WO_3 \cdot 0.33H_2O$ nano-needles. *J. Mater. Chem. C* **2018**, *6*, 2822–2829. [CrossRef]
29. An, F.; Li, X.; Min, P.; Liu, P.; Jiang, Z.; Yu, Z. Vertically aligned high-quality graphene foams for anisotropically conductive polymer composites with ultrahigh through-plane thermal conductivities. *ACS Appl. Mater. Interfaces* **2018**, *10*, 17383–17392. [CrossRef]
30. Shi, J.; Cheng, Z.; Gao, L.; Yuan, Z.; Zhao, H. Facile synthesis of reduced graphene oxide/hexagonal WO_3 nanosheets composites with enhanced H_2 sensing properties. *Sens. Actuators B Chem.* **2016**, *230*, 736–745. [CrossRef]
31. Lee, J.; Kim, S.Y.; Yoo, H.S.; Lee, W. Pd-WO_3 chemiresistive sensor with reinforced self-assembly for hydrogen detection at room temperature. *Sens. Actuators B Chem.* **2022**, *368*, 132236. [CrossRef]
32. Kumar, N.; Haviar, S.; Zeman, P. Three-layer PdO/$CuWO_4$/CuO system for hydrogen gas sensing with reduced humidity interference. *Nanomaterials* **2021**, *11*, 3456–3471. [CrossRef] [PubMed]
33. Walker, J.M.; Akbar, S.A.; Morris, P.A. Synergistic effects in gas sensing semiconducting oxide nano-heterostructures: A review. *Sens. Actuators B Chem.* **2019**, *286*, 624–640. [CrossRef]
34. Li, Z.; Huang, Y.; Zhang, S.; Chen, W.; Kuang, Z.; Ao, D.; Liu, W.; Fu, Y. A fast response & recovery H_2 gas sensor based on α-Fe_2O_3 nanoparticles with ppb level detection limit. *J. Hazard. Mater.* **2015**, *300*, 167–174.
35. Chang, S.J.; Hsueh, T.J.; Chen, I.C.; Huang, B.R. Highly sensitive ZnO nanowire CO sensors with the adsorption of Au nanoparticles. *Nanotechnology* **2008**, *19*, 175502. [CrossRef] [PubMed]
36. Zhou, R.; Lin, X.; Xue, D.; Zong, F.; Zhang, J.; Duan, X.; Li, Q.; Wang, T. Enhanced H_2 gas sensing properties by Pd-loaded urchin-like $W_{18}O_{49}$ hierarchical nanostructures. *Sens. Actuators B Chem.* **2018**, *260*, 900–907. [CrossRef]
37. Al-Hashem, M.; Akbar, S.; Morris, P. Role of oxygen vacancies in nanostructured metal-oxide gas sensors: A review. *Sens. Actuators B Chem.* **2019**, *301*, 126845. [CrossRef]
38. Kathiravan, D.; Huang, B.; Saravanan, A. Self-assembled hierarchical interfaces of ZnO nanotubes/graphene heterostructures for efficient room temperature hydrogen sensors. *ACS Appl. Mater. Interfaces* **2017**, *9*, 12064–12072. [CrossRef]
39. Zhang, L.S.; Wang, W.D.; Liang, X.Q.; Chu, W.S.; Song, W.G.; Wang, W.; Wu, Z.Y. Characterization of partially reduced graphene oxide as room temperature sensor for H_2. *Nanoscale* **2011**, *3*, 2458–2460. [CrossRef]